LA-7667-MS

Informal Report

AFATL TR-78-95

$c.3$

# Thermal Response of Explosives

# Subjected to External Heating

# LOS ALAMOS SCIENTIFIC LABORATORY

Post Office Box 1663   Los Alamos. New Mexico 87545

**UNITED STATES
DEPARTMENT OF ENERGY
CONTRACT W-7405-ENG. 36**

# Thermal Response of Explosives

# Subjected to External Heating

A. Popolato
J. J. Ruminer
A. S. Vigil
N. K. Kernodle
D. L. Jaeger

# THERMAL RESPONSE OF EXPLOSIVES
# SUBJECTED TO EXTERNAL HEATING

by

A. Popolato, J. J. Ruminer, A. S. Vigil,
N. K. Kernodle, and D. L. Jaeger

## ABSTRACT

A series of unconfined one-dimensional
heating experiments in slab geometry was con-
ducted with TNT, Comp. B, plastic-bonded HMX,
TATB, DATB, and NQ. The explosive samples
were heated on one surface at heating rates
between 10 and 25°C/min. The experimentally
determined times and temperatures to ignition
were reproduced computationally, with one
exception, by solving a one-dimensional heat-
conduction equation containing a zero-order
reaction energy source term and a time-
dependent temperature boundary condition.
The one exception was plastic-bonded NQ.
We were not able to ignite unconfined plastic-
bonded NQ under the experimental conditions
used. The heat-transfer mechanism in molten
TNT, as expected, was convective; and for
molten Comp. B, conductive. A reactive heat-
transfer program, EXPLO, was written that is
capable of solving the convective transfer
mode and accepting mixtures of explosives
reacting with first-order kinetics.

# I. SUMMARY

A series of unconfined one-dimensional heating experiments in slab geometry was performed with selected high explosives to determine the times and temperatures-to-ignition. The times and temperatures-to-ignition were computed using a finite difference solution of a one-dimensional conductive heat-transfer code with a zero-order reaction source term and the experimentally observed time-dependent boundary condition. Agreement between the experimental and computational results, using the most recently published thermokinetic data, was with one exception, within 5%.

The one exception was the NQ plastic-bonded explosive.* We were not able to completely ignite plastic-bonded NQ in the geometry tested. Our results indicated that we were pyrolyzing the explosive.

Although the heat-transfer mechanism for molten TNT was found to be convective, we were able to compute the experimentally observed times and temperatures-to-ignition to within 5%. The heat-transfer mechanism in molten Comp. B was found to be conductive.

A new heat-transfer program, EXPLO, was written to calculate the temperature as a function of time and space in a convective medium and the ignition temperatures of explosive mixtures under conditions of very slow heating or prolonged exposure to temperatures near the critical temperature.


# II. INTRODUCTION

All chemical high explosives are metastable chemicals and decompose exothermally at all temperatures. If the decomposition kinetics are known, then it should be possible to compute the temperatures and times-to-ignition as a function of the geometry of the explosive and the time-dependent boundary conditions. The ability to compute these parameters with confidence is important in all aspects of operational safety, including the manufacture, storage, and delivery of explosive ordnance. Accidental initiation of explosives by mechanical impact is, in the limit, a problem of thermal initiation followed by thermal conduction and eventual growth. The storage life of explosive mixtures is a problem related to thermal decomposition. Explosive

---

*95 wt% NQ/5 wt% Estane

2

ordnance exposed to various thermal environments (in particular, aerodynamic heating in supersonic flight) represents another important area dealing with thermal ignition.

Previously published papers on the thermal ignition of explosives[1-5] have pointed out the strong dependence of time-to-ignition on the geometry of the explosive and the boundary temperature. In all these experiments, the time-to-ignition was measured in terms of the sudden rupture of a container or the disassembly of the heating apparatus. The temperature of the explosive sample was never actually determined; it was always assumed to be the same as the temperature of the material surrounding the explosive or the container.

Zinn and Mader[2] and later Zinn and Rogers[4] were the first to correlate theoretical calculations based on transient reactive heat conduction with isothermal experiments. Results of their experiments and computations indicate that the uncertainties in the available thermokinetic data were sufficient to overshadow the uncertainties in other parameters, such as time and temperature. Considering these problems, reasonable agreement was obtained between the theory and the experiments.

The purpose of this program was to theoretically and experimentally study the response of selected high explosives to a predetermined time-dependent boundary condition. A one-dimensional test configuration was chosen to simplify both the experiments and calculations.

In most practical problems of thermal ignition, the parameters of concern are the time and temperature-to-ignition. The variation of temperature with time, in a reactive explosive, is described by the following expression:[2]

$$\rho C \frac{\delta T}{\delta t} = k \nabla^2 T + \rho Q Z e^{-E/RT} . \tag{1}$$

For configurations having one-dimensional symmetry such as slabs, cylinders, or spheres, the Laplacian operator $\nabla^2$ in equation (1) takes the form:

$$\frac{\delta^2}{\delta r^2} + \frac{m}{r} \frac{\delta}{\delta r} . \tag{2}$$

The integer m has the value of zero for slabs, one for cylinders, and two for spheres. Substitute equation (2) into (1) and we find:[6]

$$\rho C \frac{\delta T}{\delta t} = k\left[\frac{\delta^2 T}{\delta r^2} + \frac{m}{r}\frac{\delta T}{\delta r}\right] + \rho Q Z \ e^{-E/RT}. \tag{3}$$

The variables in equation (3) are:

$T$ = absolute temperature

$r$ = distance coordinate

$t$ = time

$\rho$ = density

$C$ = heat capacity

$k$ = thermal conductivity

$E$ = activation energy

$Z$ = frequency factor

$Q$ = heat of decomposition

$R$ = gas constant

The energy-source term in equation (3) represents zero-order reaction kinetics. This is a simplified approximation of the normal decomposition process and does not take into account the depletion of the explosive through reaction. Under conditions of rapid heating where ignition occurs at the surface of the explosive, ignition takes place before much of the explosive has decomposed, and a zero-order term adequately describes the energy source.[4]

A one-dimensional finite difference code, TEPLO,[6] was written to solve equation (3). TEPLO treats problems of layered media with a constant temperature-boundary condition in slab, cylindrical, or spherical geometry. For this study, TEPLO was modified to accept time-dependent boundary conditions.

The details of this modification, including a sample problem, are given in the Appendix.


III. EXPERIMENTAL PROGRAM

The accuracy of calculated values for either the time-to-explosion or the critical temperature of high explosives depends upon the validity of the thermokinetic data used in the calculations. We conducted a series of transient heat-conduction experiments in one-dimensional slab geometry to verify

the validity of transient heat-transfer calculations using energy-contributing source terms. This geometry was chosen to simplify the calculation and the experiment.

## A.    Description of Test Assembly

A schematic diagram of the test assembly is shown in Fig. 1. The assembly is designed to provide a time-dependent, uniform temperature on one surface of a slab of explosive and to determine the temperature in the explosive as a function of time and space. Since the diameter of the sample is large relative to the height, and the system is well insulated, heat losses through the sides are minimized and heat flow should be nearly one-dimensional.

The heater plate was fabricated from cast, series 600, aluminum tool plate, 15.9 mm thick. This alloy of aluminum was chosen because it is more thermally stable than the other alloys. Eight, 250-W, resistance strip heaters, 203 mm long and 25 mm wide, were mounted in parallel on one surface of the aluminum tool plate. The heaters were sized to provide the capability of raising the temperature of the aluminum plate from room temperature to 300°C in 15 min. A schematic diagram of this assembly is shown in Fig. 2.
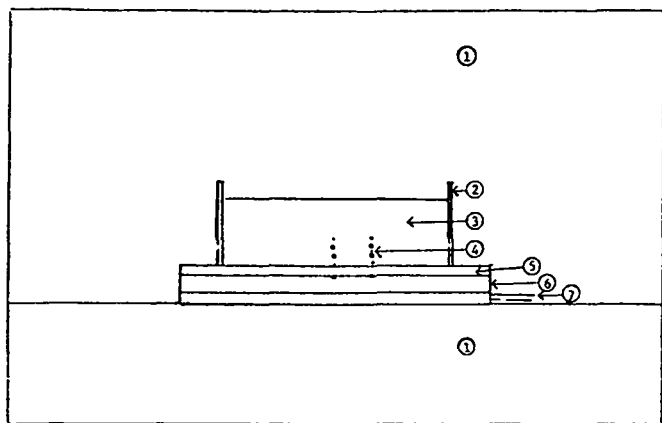


Fig. 1.  Thermal response test assembly schematic.
   1.  Gas foam insulation
   2.  Sample holder tube
   3.  Test sample
   4.  Thermocouples
   5.  Sample holder base plate
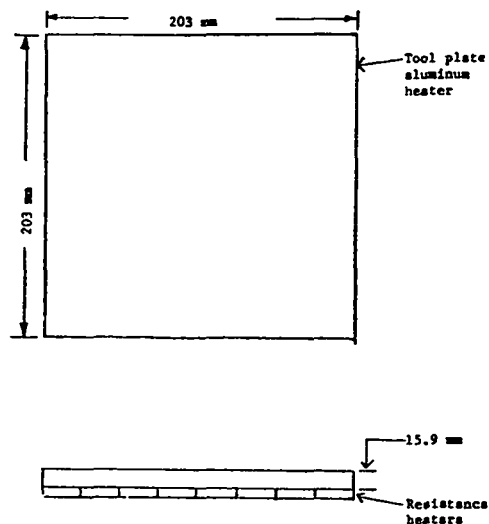   6.  Heater plate
   7.  Heater



Fig. 2.  Heater plate assembly.

To obtain an estimate of the temperature gradients we would experience during an experiment, a sheet of aluminum tool plate 6.35 mm thick was placed over the heater plate. This plate was used to simulate the sample holder base plate. Five, 30-gage, Chromel-Alumel thermocouples were mounted on the surface opposite the heater plate. One thermocouple was located in the center, and two were located 25.4 mm from the center and separated by 90°. The other two were located 50.8 cm from the center and were also separated by 90°.

Experimental runs were made to determine the temperature spread on the aluminum surface, with the center of the surface maintained at 105 and 300°C, respectively. The maximum temperature spread over the surface area sampled was less than 2°C. The surface of the plate did not warp, remaining plane within 0.050 mm, at the two test temperatures (105 and 300°C). There was no change in planarity after the temperature of the plate was returned to ambient.

A phenolic-bonded, fiber-glass tube, 152 mm o.d. and 140 mm i.d. mounted in a groove milled in the surface of the 6.35-mm-thick aluminum tool plate, was chosen to hold TNT-based explosive samples. This tube material was chosen because it has about the same thermal conductivity as the high explosive and can withstand exposure to 300°C. RTV silicone was used to bond the tube to the aluminum plate and to hold the sample in place after the phase transition. Ten, 30-gage, Chromel-Alumel thermocouples were mounted in the container. Five of the thermocouples were mounted on the center line of the tube. The first thermocouple was mounted on the surface of the sample holder base plate, and the remaining four were mounted a nominal 6.35 mm above each other. Five additional thermocouples were mounted 25.4 mm from the center line to check the validity of our one-dimensional heat flow assumption. All the thermocouples were mounted through holes drilled in the wall of the tube. RTV silicone rubber was used to plug the holes so that the thermocouples could move, because the coefficient of expansion of the metal is much less than that of the explosive. The explosive was cast into the container after the thermocouples were mounted, and the exact location of the thermocouples was determined radiographically. The sample holder is shown schematically in Fig. 3.

The experimental arrangement used for the plastic-bonded explosives was modified because these explosives do not have solid-liquid phase transitions. We used discs of these materials that were 152 mm o.d. and 6.35 mm high. Slots 0.38 mm wide and 0.38 mm deep were milled on one surface of each disc
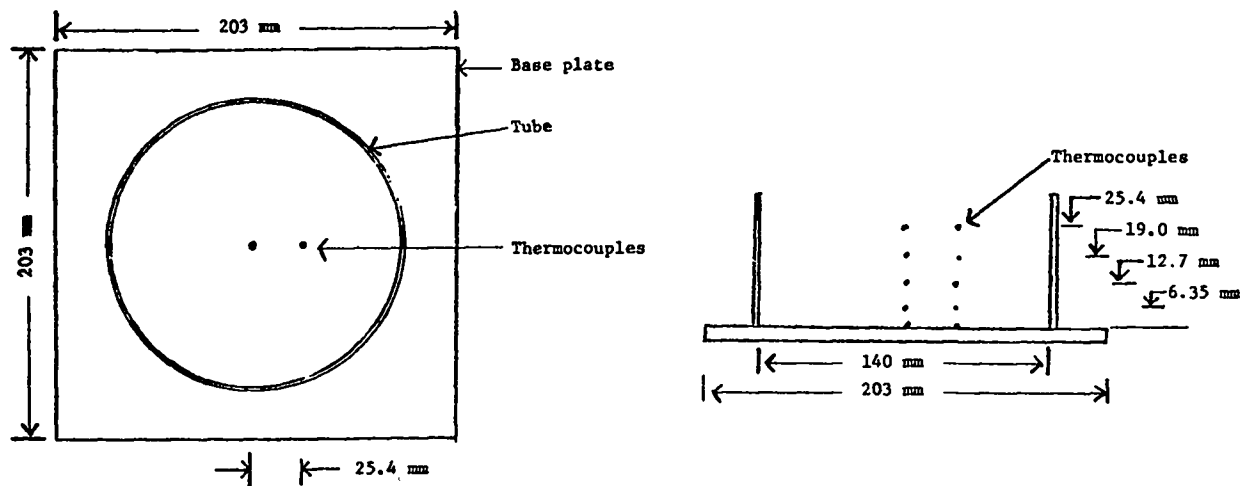
Fig. 3. Sample holder assembly.

to accommodate the thermocouple wires. Five discs were assembled with thermocouples placed on the center line and 25.4 mm off the center line. A silicone foam disc was placed over the top of the explosive, and the assembly was clamped to the aluminum base plate with a phenolic plate and four bolts.

A schematic of this assembly is shown in Fig. 4.

This configuration provided good contact between the heater plate and the explosive during the heating cycle. The locations of the thermocouples were precise.

B.    Calibration Experiments

Before experimenting with explosives, we decided to perform two calibration experiments with nonreacting materials. The purpose of these experiments was to determine whether we could match the experimentally observed heat flow with TEPLO for a nonreacting material with and without a solid-liquid phase transition. These experiments would also provide some data on the errors we could expect in measuring the temperature and the location of the thermocouples in the samples.

A castable polyurethane, CPR-1009 manufactured by the Upjohn Company, was chosen as the test material for the no-phase-transition test. This material was chosen because it has about the same thermal conductivity and expansion coefficient as the high explosives.

Results of the first experiment, in which the sample holder base plate was heated from ambient to 105°C in 10 min and held constant, are shown in
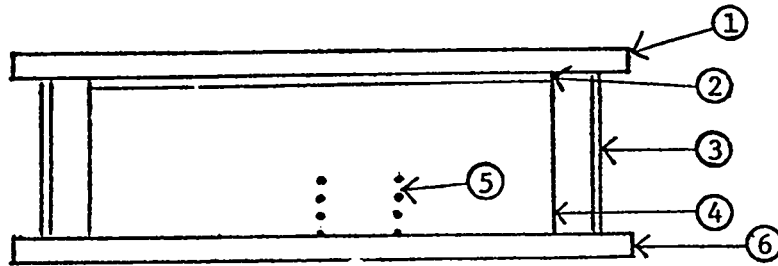
Fig. 4.  Thermal response test assembly schematic
         for plastic-bonded explosives.
         1.  Phenolic cover plate
         2.  Silastic cushion
         3.  Tie rods
         4.  HE sample
         5.  Thermocouples
         6.  Aluminum base plate

Fig. 5.  The upper curve is a plot of the temperatures at the center and
25.4 mm from the center, at the plastic-sample holder base plate interface.
At this surface, the temperature difference between the two thermocouples
was less than 0.25°C.  The other four curves in Fig. 5 are plots of tempera-
ture as a function of space and time.  The locations of the thermocouples
with respect to the sample holder base plate were determined from radiographs
taken after the plastic sample was cast over the thermocouples.  These results
indicated that heat flow, through a central core roughly 50 mm in diameter,
was one-dimensional.

A transient heat-flow calculation was performed with TEPLO imposing the
experimentally observed time-dependent boundary condition shown in Fig. 5.
Results of this calculation and the experimentally observed temperatures are
shown in Fig. 6.

At late times (>60 min), the calculated temperature matches the experi-
mentally observed temperature for all the locations.  At early times, the dif-
ference between calculation and experiment at a depth of 19 mm is about 6% in
time for a given temperature profile.  This difference could be caused by
errors of 5% or less in either the location of the thermocouple or the thermal
diffusivity of the material.  The error in locating the position of the ther-
mocouple relative to the sample holder base plate was estimated to be ±0.25 mm.
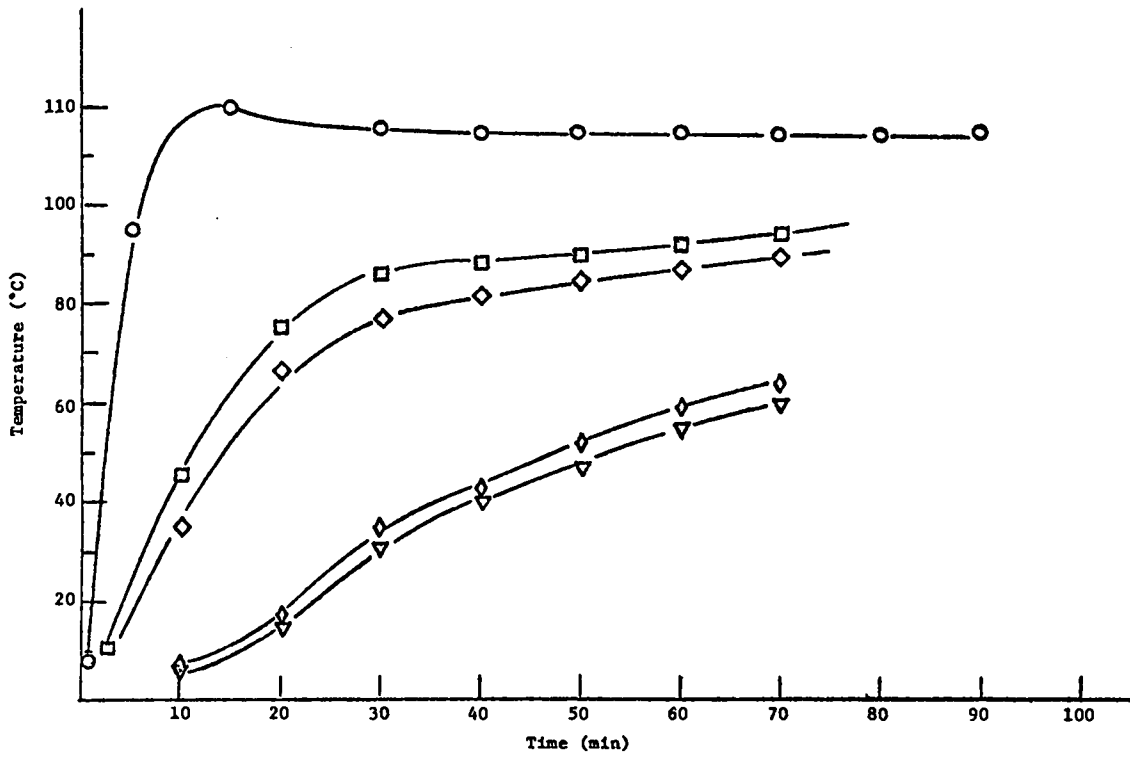
8

Fig. 5.   CPR-1009 calibration run, experimental results.
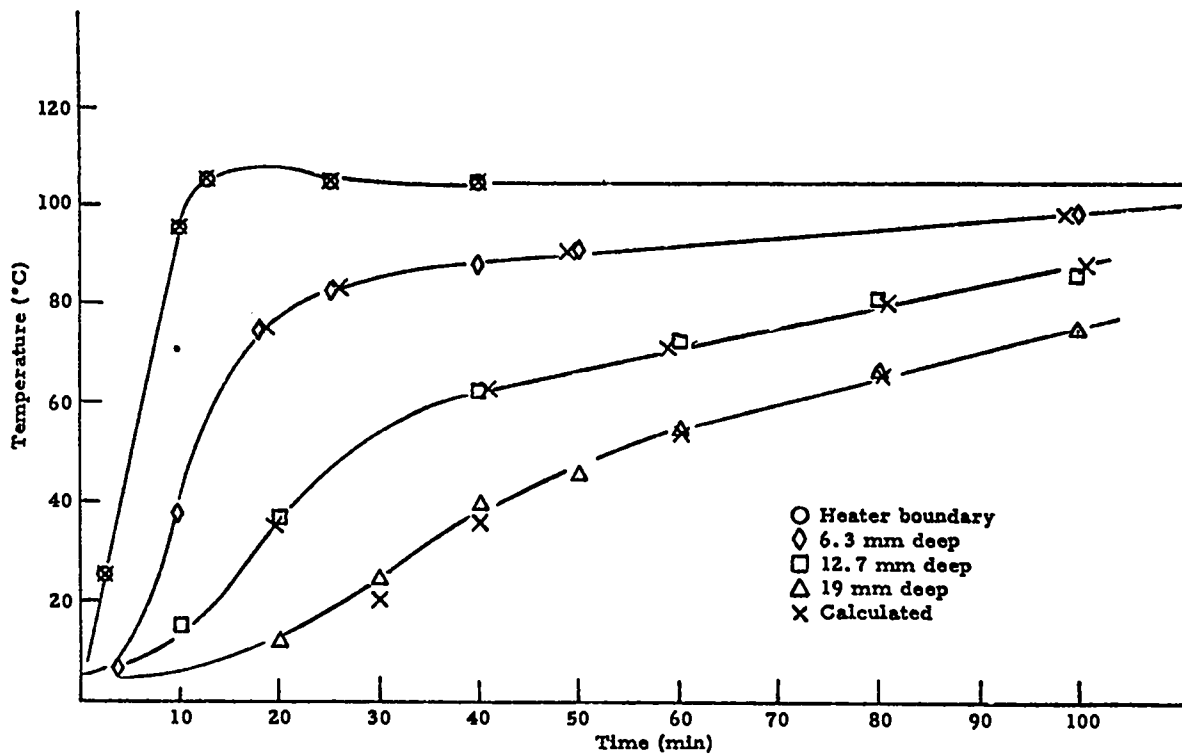


Fig. 6.   CPR-1009 calibration curve, experimental and calculated.

9

To determine the effect of a solid-liquid phase transition, a calibration experiment was conducted with stearic acid, which melts at 60°C. The experimental results are shown in Fig. 7.

The obvious feature of this result is that the temperature of the liquid phase, a short time after melting, is uniform throughout the bulk of the liquid. This indicates that the heat-transfer mechanism in the liquid phase is convective and not conductive. This mode of heat transfer cannot be handled by TEPLO.

## C.    Transient Heat-Conduction Experiments

1. TNT. Two experiments were conducted with TNT. In the first, the temperature at the sample holder base plate-explosive interface was increased at the rate of 10°C/min to 100°C and then maintained at 100°C.

Experimental results for TNT are presented in Fig. 8. Obviously, the heat-transfer mechanism in the liquid phase is convective. The temperature of the bulk of the liquid TNT is approximately half way between the boundary temperature and the melting point of TNT. Note the similarity between the TNT result and the results obtained with stearic acid. These data indicate that we have a large gradient in a thin boundary layer at each interface.
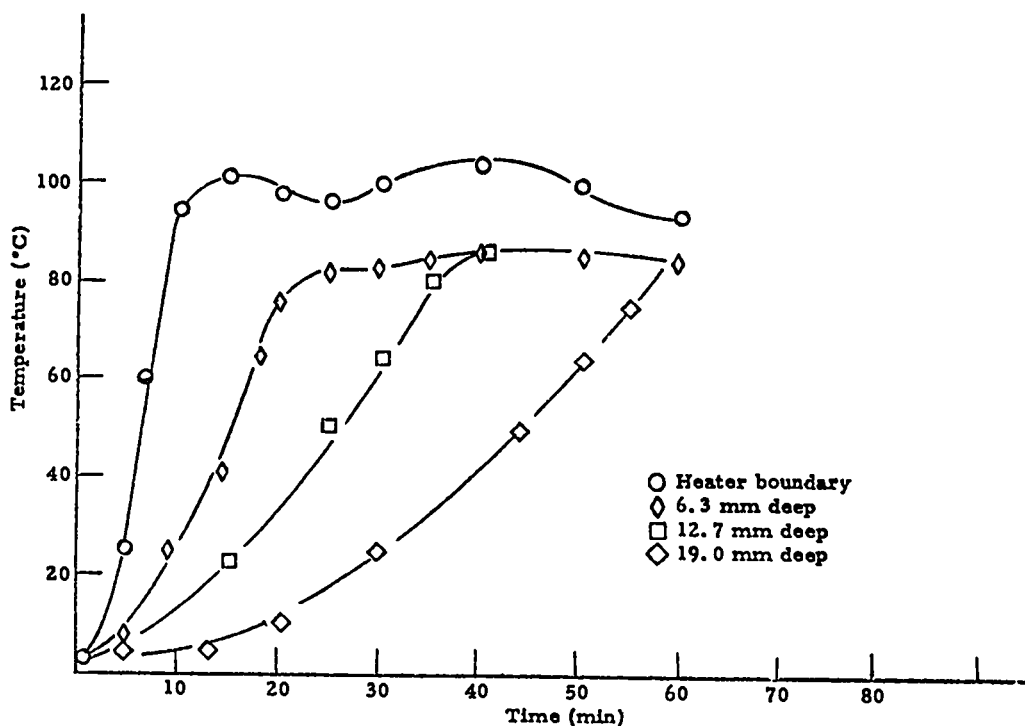
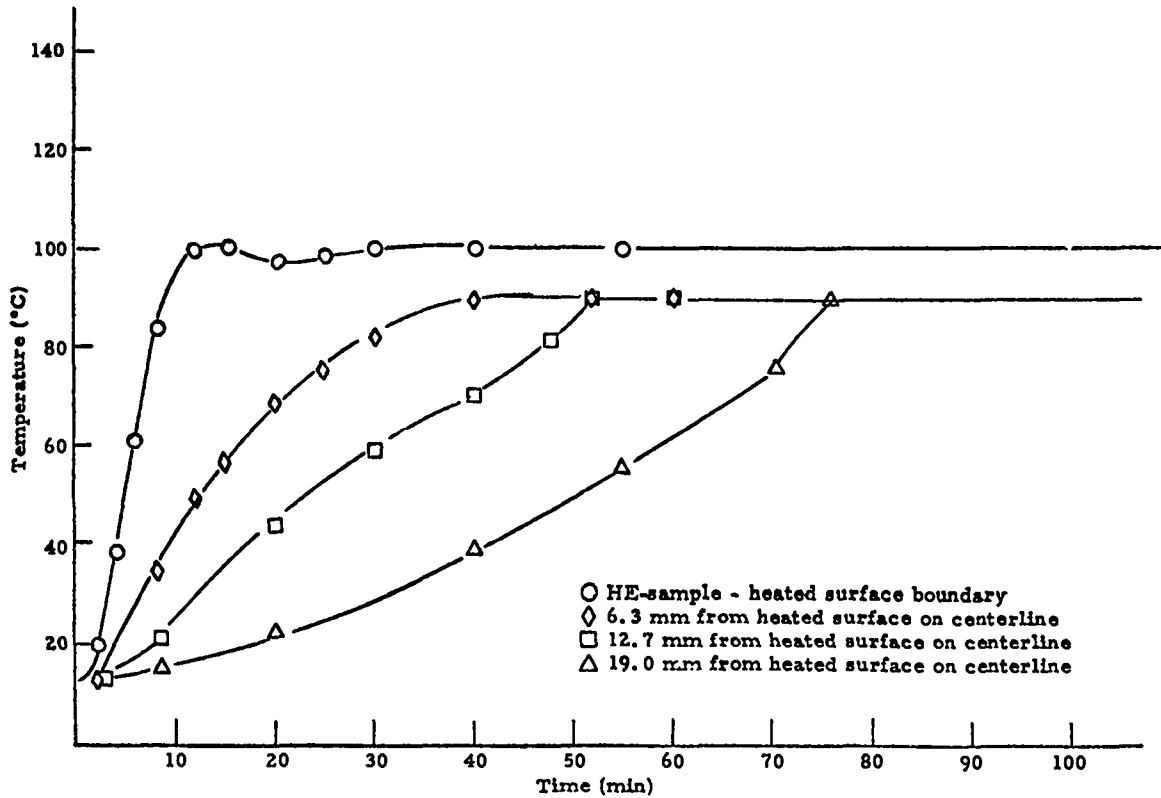Fig. 7.   Stearic acid calibration curve, mp 60°C.

Fig. 8. TNT, boundary temperature 100°C, heating rate 10°C/min.

The thickness of the boundary layer should be related to the viscosity of the fluid and the temperature difference between the hot surface and the melt temperature. A schematic representative of the temperature in the TNT as a function of space after 70 min of heating is shown in Fig. 9.

In the second TNT experiment, the temperature at the sample holder base plate-explosive interface was increased at the rate of 17°C/min.

A graph of the experimental and calculation results for this experiment is presented in Fig. 10. The time-dependent boundary temperature imposed on the calculation was the experimentally obtained temperature at the explosive-aluminum interface through the first 10 min of heating followed by a constant 17°C/min increase beyond 10 min. Thus, the calculation was forced to agree with the experiment at this interface, and any temperature increases in TEPLO greater than 17°C/min at times longer than 10 min would represent a contribution from the energy source term $QZ\ e^{-E/RT}$. After a heating period of 16 min, the calculated temperature in the first explosive cell at the explosive-aluminum interface (using the kinetics listed in Table I) was greater than
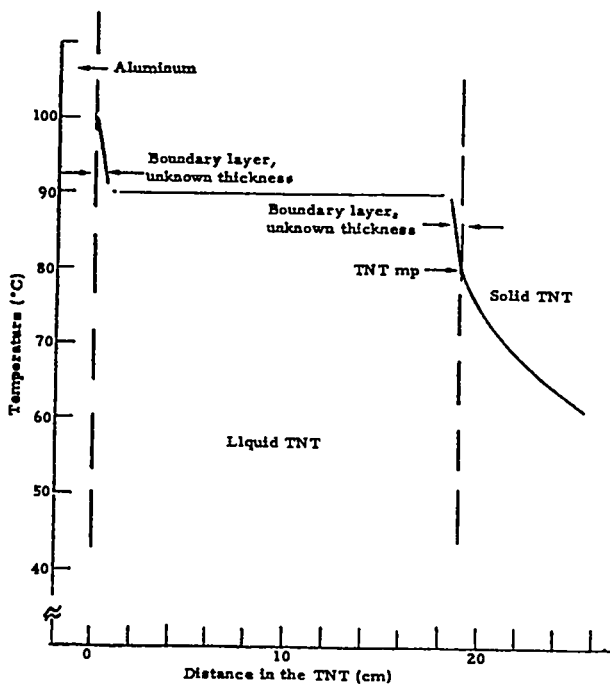
11

Fig. 9.  TNT, boundary temperature
100°C, temperature after
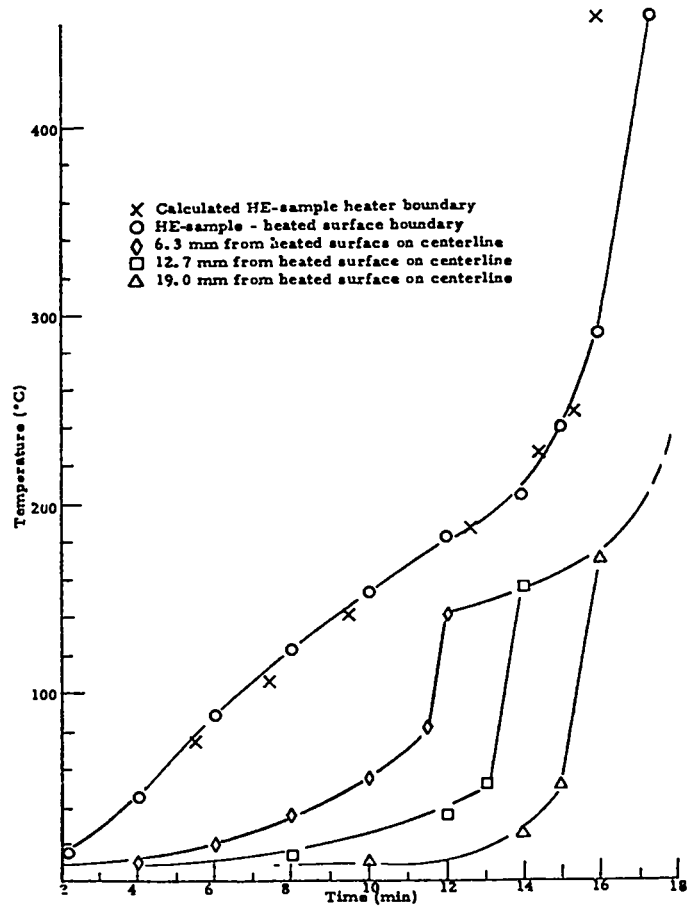70 min of heating.

Fig. 10.  TNT, heating rate 17°C/min.

1000°C, and the experimentally observed temperature was 290°C.  The excellent agreement between the experiment and the calculation indicates that a stagnant layer existed at the boundary.  At the time ignition occurred (16 min), more than 19 mm of the TNT was liquid and at a uniform temperature roughly half way between the boundary temperature and the melt temperature.  The temperature profile in the TNT just before ignition is schematically shown in Fig. 11. These results indicate that the thickness of the stagnant layer under these conditions is sufficient to start an ignition.  It is quite possible that the application of external forces such as vibration, or larger temperature gradients, could decrease the layer thickness and therefore change the ignition times and temperatures.

## TABLE I

### THERMOKINETIC PARAMETERS USED IN TEPLO CALCULATIONS

| Material | Source of Z and E | $\rho$ g/cm$^{-3}$ | Tm °C | H (Fusion) cal/g | Cp cal/g °C (s) | Q cal/g | Z sec$^{-1}$ | E kcal mol$^{-1}$ | $\lambda \times 10^4$ cal cm$^{-1}$s$^{-1}$°C$^{-1}$ |
|---|---|---|---|---|---|---|---|---|---|
| TNT | a | 1.60 | 80 | 24 | $0.26 + 8.4 \times 10^{-4}T$ | 500 | $2.51 \times 10^{11}$ | 34.4 | 6.2 |
| Comp. B (RDX) | a | 1.72 | 80 | 10 | $0.23 + 1.03 \times 10^{-3}T$ | 500 | $2.44 \times 10^{16}$ | 43.1 | 5.0 |
| | b | | | | | | $3.16 \times 10^{18}$ | 47.5 | |
| | c | | | | | | $2.0 \times 10^{17}$ | 43.1 | |
| PBX 9501 (HMX) | a | 1.83 | 250 | 50 | $0.23 + 8.6 \times 10^{-4}T$ | 500 | $6.37 \times 10^{18}$ | 51.3 | 10.7 |
| | c | | | | | | $6.37 \times 10^{18}$ | 52.0 | |
| PB TATB | d | 1.89 | -- | -- | $0.21 + 1.32 \times 10^{-3}T$ | 500 | $3.5 \times 10^{19}$ | 59.9 | 9.5 |
| PB DATB | d | 1.74 | 286-290 | -- | 0.261 | 300 | $1.17 \times 10^{15}$ | 46.3 | 6.0 |
| PB NQ | d | 1.70 | -- | -- | 0.26 | 500 | $2.84 \times 10^7$ | 20.9 | 5.0 |

[a]R. N. Rogers, private communication

[b]A. J. B. Robertson, Ref. 8

[c]Empirical changes used to match experimental data

[d]R. N. Rogers, Ref. 7

2. Composition B. To determine the heat-transfer mechanism in molten Comp. B, a preliminary heating test was conducted in which the temperature at the explosive-heater plate interface was increased at the rate of 10°C/min to 100°C and then maintained at 100°C. The experimental and calculational results obtained are shown in Fig. 12. The excellent match between experiment and calculation indicates that the heat-transfer mechanism is primarily conductive and that the heat-transfer coefficients we used are relatively accurate. The major difference in physical properties between TNT and Comp. B at temperatures above the melting point of TNT is the viscosity. At 85°C, the viscosity of TNT is approximately 0.1 to 0.12 P, and the viscosity of the Comp. B slurry is 5 to 10 P. Because the thermal diffusivities of the two explosives are approximately the same, the difference in heat-flow mechanisms can most likely be attributed to the viscosity.

Following this experiment, three experiments were performed with Comp. B at heating rates of 13, 17, and 23°C/min, respectively. Results obtained in
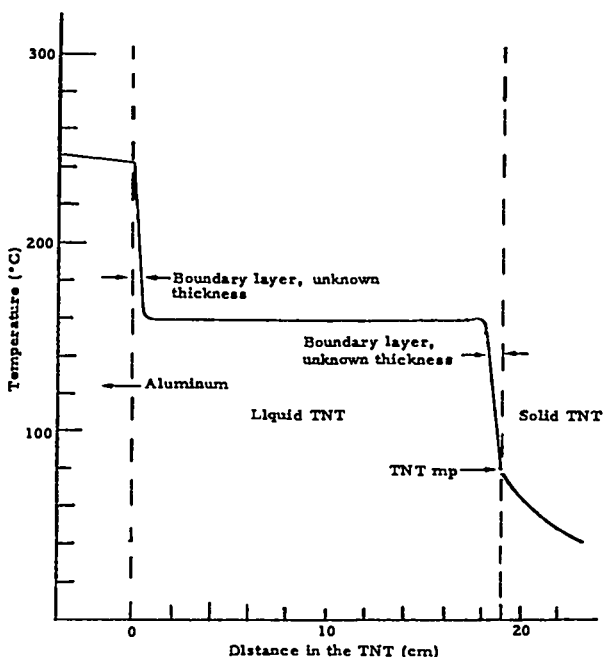
Fig. 11.   TNT, heating rate ~17°C/min, temperature profile after 15 min of heating.
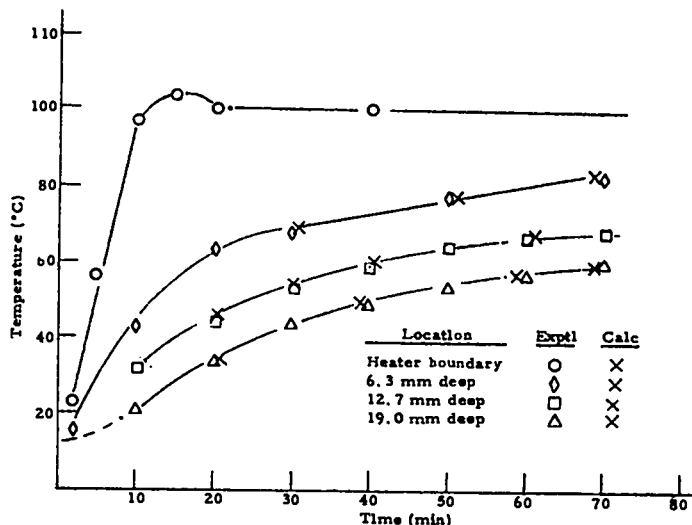
Fig. 12.   HE heating, Comp. B, boundary temperature 100°C, heating rate 10°C/min.

14

these experiments are shown in Figs. 13-15. At the lowest heating rate (13°C/min), the kinetic of Rogers[7] and Robertson[8] predict a slightly higher ignition temperature than the experiment. The parameters used in the calculations are listed in Table I.

At a heating rate of 23°C/min, we obtained a better computational match to the experiment with RDX kinetics provided by Rogers. This result implies that the decomposition rate of RDX is increased as it dissolved in TNT and contradicts the observations made by Robertson[8] that the decomposition rate of RDX decreases when it is dissolved in TNT. Robertson's explanation for the decrease in decomposition rate of RDX in solution was based on a short chain-reaction decomposition mechanism. Thus, as the explosive molecules
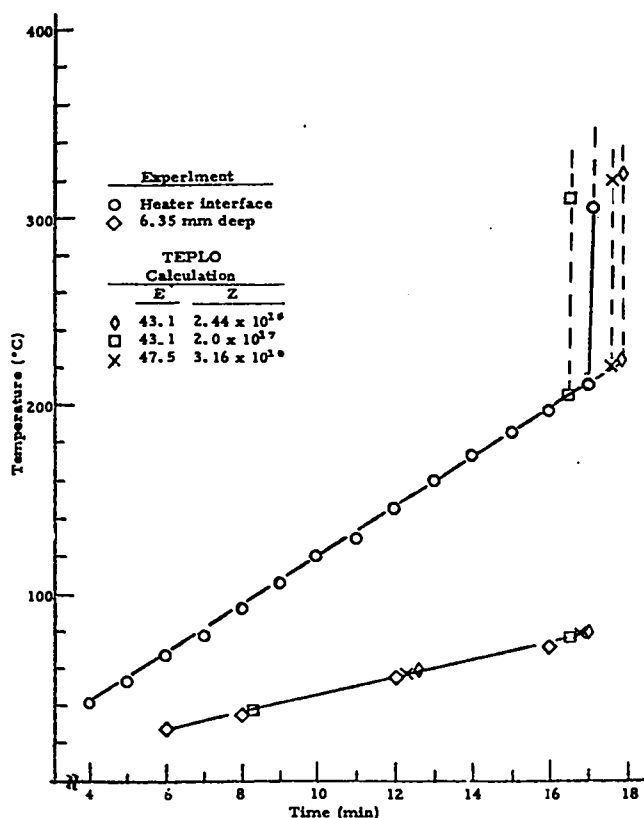


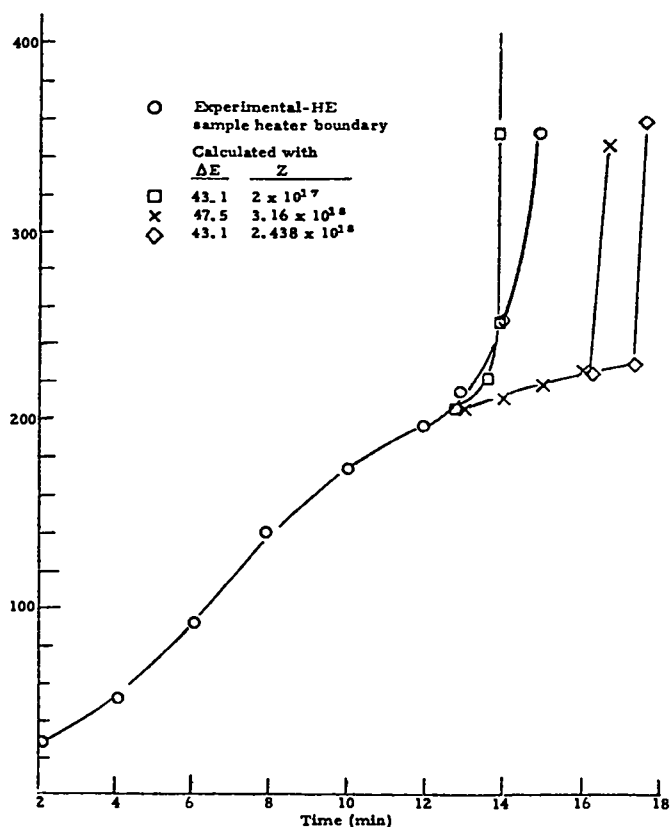Fig. 13. Comp. B, heating rate 13°C/min.

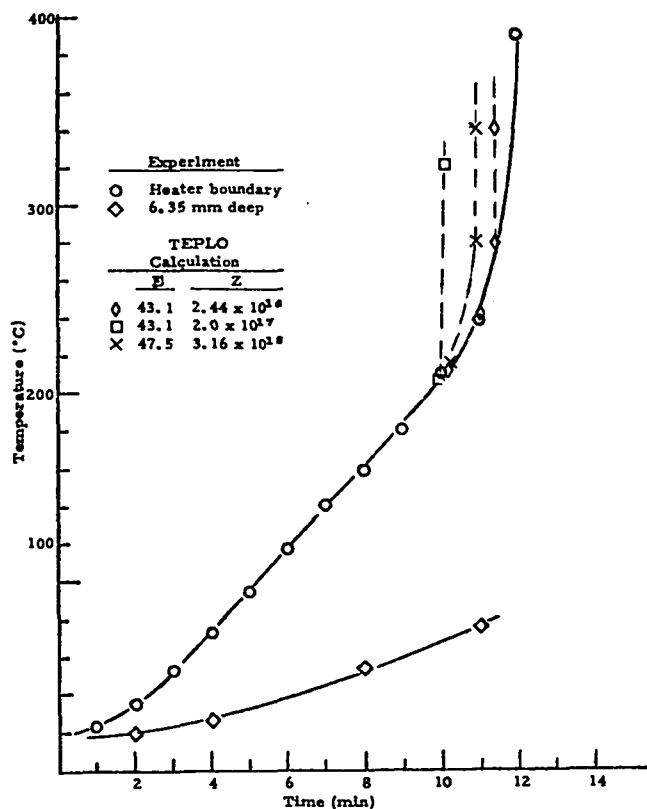Fig. 14. Comp. B, heating rate 17°C/min, HE sample-heater boundary.

Fig. 15. Comp. B, heating rate 23°C/min.

were separated by inert solvent, the chain development was increasingly inhibited. In a series of experiments that were performed isothermally, over the temperature range of 200 to 280°C, Robertson found that TNT behaved as an inert solvent.

A possible mechanism for the apparent increase in RDX reaction rate has been suggested by Rogers.[9] He suggested the possibility of a series of chain-type reaction between the TNT and RDX producing intermediate products that could either decompose exothermally or catalyze the direct decomposition of RDX. At low heating rates or at prolonged exposure to lower temperatures, there would be some time available for the reaction of RDX with TNT and for intermediate products to either decompose or catalyze the decomposition of RDX. The mechanism suggested by Rogers has never been experimentally verified.

3. Plastic-Bonded HMX (PBX 9501*). Results obtained in a heating experiment with PBX 9501 are presented in Fig. 16. An excellent match between the experiment and the TEPLO calculation, using the parameters listed in Table I, was obtained for the temperature as a function of time and space along the center line of the explosive sample 6.35, 12.70, and 19.0 mm from the sample-heater interface. This verifies that the thermal diffusivity for PBX 9501 used in TEPLO is correct. The experimental time and temperature-to-ignition is slightly higher and longer than time and temperature computed with TEPLO using the HMX kinetics of Rogers.[7] A slightly better match is obtained if

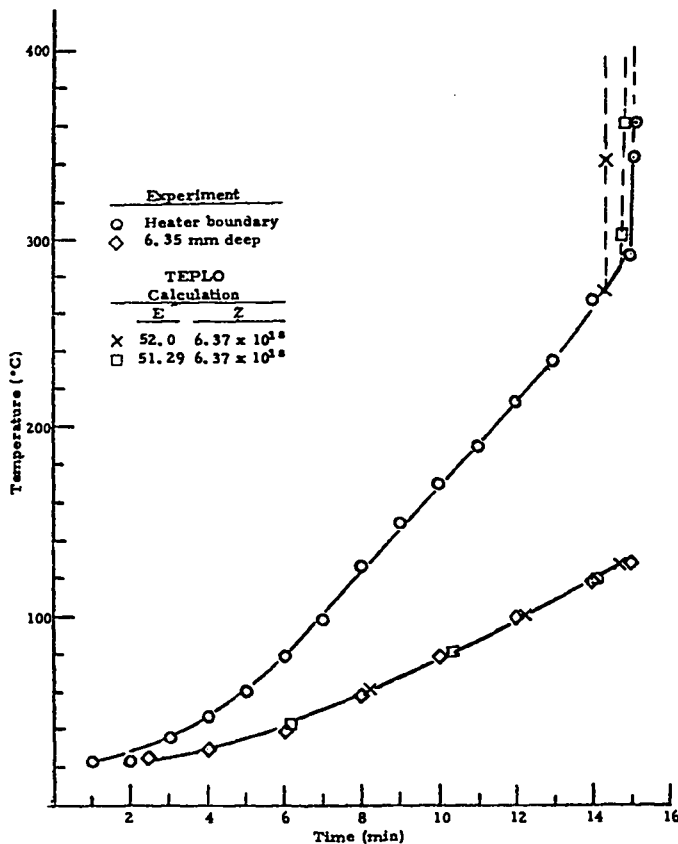*95 wt% HMX, 2.5 wt% Estane, 2.5 wt% nitroplasticizer

16

Fig. 16. PBX 9501, heating rate 22°C/min.

the activation energy is reduced from 52.0 to 51.3 kcal/mol. With either set of kinetics, the agreement between the experiment and the calculation is very good from a practical standpoint.

### 4. Plastic-Bonded TATB (PBX-9502*).

The experimental and calculational results obtained with PBX 9502 are shown in Fig. 17. The agreement is excellent between the experiment and the time and temperature-to-ignition using the values in Table I. Our value for the thermal diffusivity seems to be slightly in error because the experimentally observed "nonreactive" heat transfer is greater than the calculated value. An extraordinary feature of this experiment is that the thermocouple leads 6.35 mm from the heated surface survived long enough to obtain an estimate of the burning rate. The stick-burning rate is approximately 3 mm/min.

### 5. Plastic-Bonded DATB.

A single, unconfined, one-dimensional, heating experiment was run with a Viton A-bonded DATB sample consisting of 5 wt% Viton A and 95 wt% DATB. In this experiment, the temperature at the sample holder base plate was increased at the rate of 20°C/min. The experimental and computational results are shown in Fig. 18. The DATB parameters used in the calculations are listed in Table I. In the experiment, runaway reaction started approximately 10° lower and 1 min sooner than the calculation predicts.

We were not able to calculate the experimentally observed temperature as a function of time and space along the center line of the nonreacting region
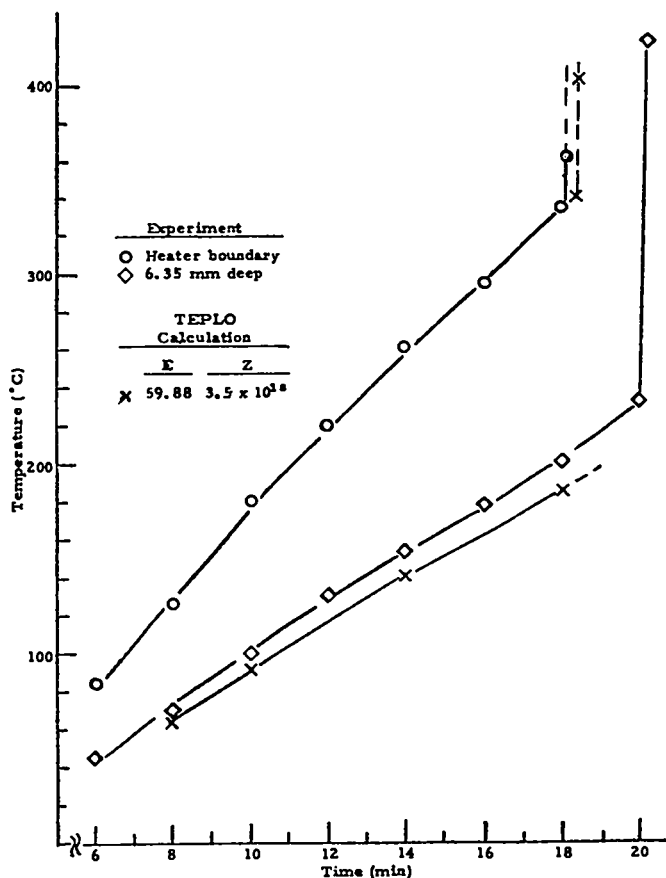
---

*95 wt% TATB, 5 wt% Kel-F 800

Fig. 17.  PBX 9502, heating rate 20°C/min.
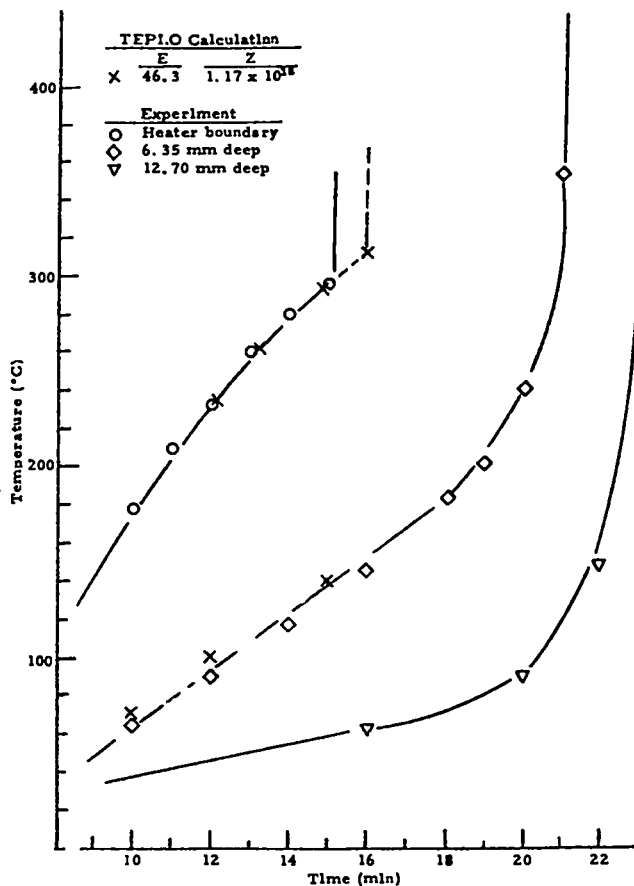
Fig. 18.  95 wt% DATB, 5 wt% Viton A, heating rate ~20°C/min.

of the charge.  The calculated temperature is, on the average, a few degrees higher than the experimentally observed temperature.  This difference indicates that we have a small error in either the thermal conductivity or the heat capacity.  Since the error is very small, we did not attempt to redetermine these parameters.

6.  Plastic-Bonded NQ.  Two, unconfined, one-dimensional, heating experiments were run with Estane-bonded NQ samples consisting of 95 wt% NQ and 5 wt% Estane.  The first run was performed at a heating rate of about 20°C/min and the second at 10°C/min.  The experimental results obtained in both runs were unexpected.  At the conclusion of both NQ runs, the glass foam used to insulate the assembly was almost intact, and, in the space previously occupied by the plastic-bonded NQ, we found a residue that appeared to be a low-density

18

Fig. 19.  NQ residue after burn.

carbon foam with almost the same dimensions as the starting materials. Figure 19 is a photograph of the residue. The aluminum plate used to hold the sample was deformed and partially melted. In all previous experiments with RDX-, HMX-, TATB-, and DATB-based explosives, all the explosive material was consumed and the temperatures were high enough to melt and deform the foamed glass insulation.

The experimental and computational results for the runs conducted at heating rates of 10 and 20°C/min are presented in Figs. 20 and 21, and the thermokinetic constants used in the calculations are given in Table I. In neither run did we observe the temperature excursion predicted by the calculation.

The residue was sampled and analyzed for carbon, hydrogen, and nitrogen. Results of this analysis are listed in Table II and compared with those for NQ. From these data, normalized to C, we can derive an empirical formula for the residue as $CH_{1.13}N_{1.26}O_{0.07}$. If we assume that this composition is representative of the residue, then it represents the NQ ($CH_4N_4O_2$) partially burned to produce 1 mole of water and some nitrogen or oxide of nitrogen, or, in other words, an incomplete pyrolysis has taken place. The net energy change in going from NQ to NQ less 1 mole of water should be small, and this could account for the absence of a temperature excursion. The exclusion of air and its potential contribution to the oxidation reaction could be explained by the fact that the foamed glass surrounding the assembly was well sealed and was not disturbed during the pyrolysis.

TABLE II

RESIDUE ANALYSIS

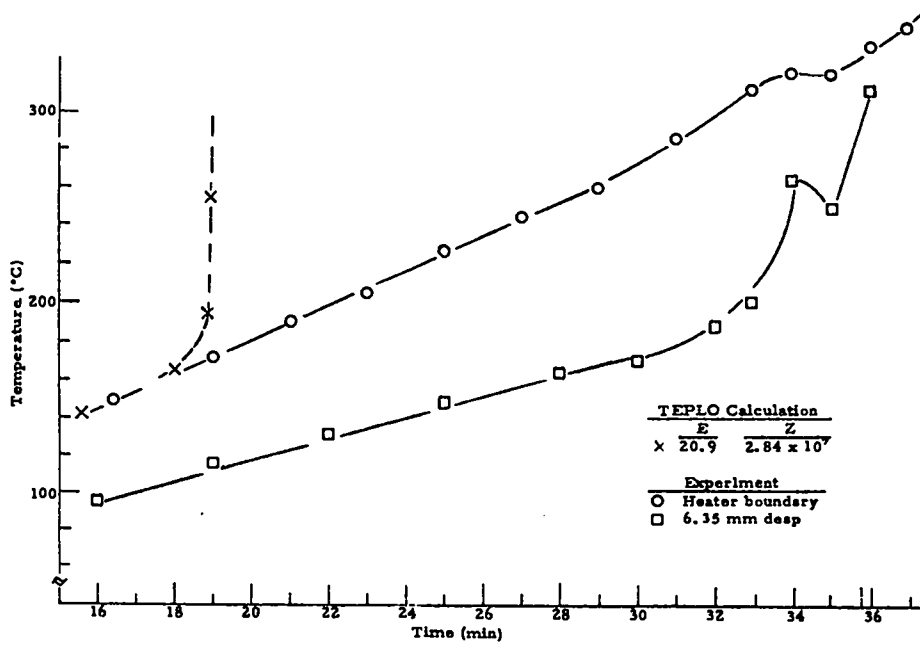| Material | Elemental Analysis (wt%) | | | |
|---|---|---|---|---|
| | C | H | N | O |
| Residue from burn | 37.9 | 3.4 | 55.2 | 3.5[a] |
| NQ[b] | 11.5 | 3.9 | 53.8 | 30.8 |

[a]By difference
[b]Theoretical

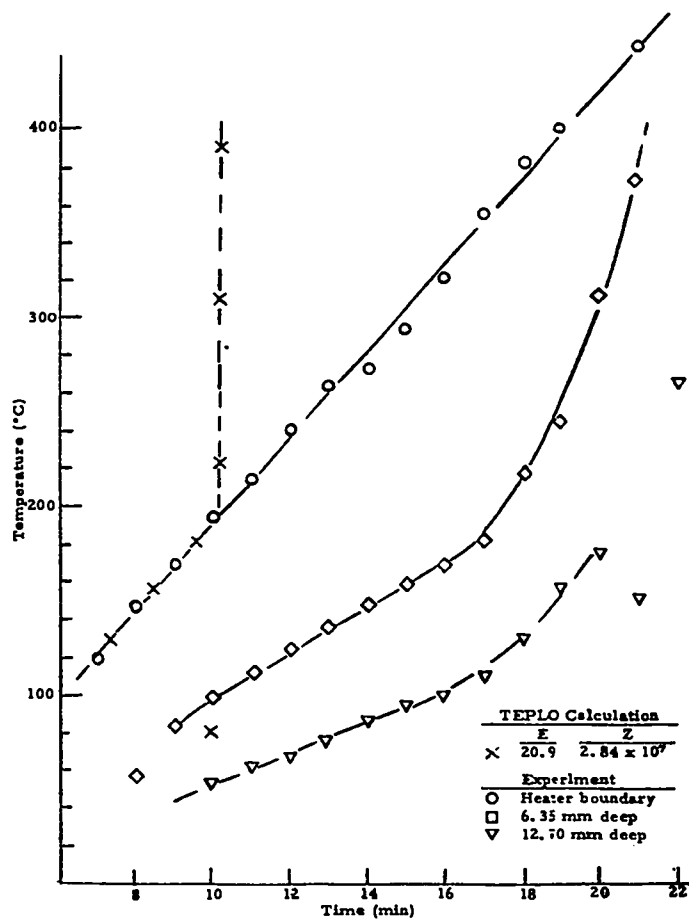Fig. 20.   95 wt% NQ, 5 wt% Estane, heating rate 10°C/min.



Fig. 21.   95 wt% NQ, 5 wt% Estane, heating rate ~20°C/min.

A series of thermal stability tests was run to obtain more information on the thermal stability of NQ. Results obtained in the modified Henkin test for low- and high-bulk-density NQ are presented in Fig. 22. These data indicate that the critical temperature of high-bulk-density NQ is slightly lower than that of the low-bulk-density material. Furthermore, a significant observation was made while conducting these experiments: No explosions or violent reactions were obtained. The decomposition reaction was a mild gas evolution that eventually ruptured the gas seal, without explosive force.

Thermogravimetric analysis (TGA) was performed with NQ and a few other explosives of military interest. Results of this analysis are presented in Fig. 23. These data indicate that a decomposition reaction starts at temperatures between 180 and 190°C for NQ and that approximately 18% of the NQ remains as a residue.

## IV. TRANSIENT REACTIVE HEAT FLOW IN CONDUCTIVE AND CONVECTIVE SYSTEMS

A finite difference program has been developed to calculate the temperature fields and times-to-initiation for explosive materials. This program, called EXPLO, was derived from TEPLO.[6] A detailed description of the capabilities of EXPLO with a few sample problems and a users' guide have been published by D. L. Jaeger.[10] It was designed to correct some of the minor deficiencies in TEPLO and to expand the range of heat-transfer modes.

The major differences between TEPLO and EXPLO are the following:

1.  The energy-source term in EXPLO is designed to handle first-order kinetics with not more than five such energy-generating materials.
2.  EXPLO has a routine to handle either free or forced convection.

Inclusion of first-order kinetics with multiple-source terms provides the capability of determining, with mixed explosives, the depletion rate of each explosive component or the rate-determining explosive. This feature is useful under conditions of slow heating or exposure to temperatures near the critical temperature. Under these conditions, it is possible to deplete small quantities of the more reactive materials or to have these materials dominate in the initiation mechanism.

The convection routine makes it possible to compute the temperature as a function of space and time in materials that undergo a solid-liquid phase
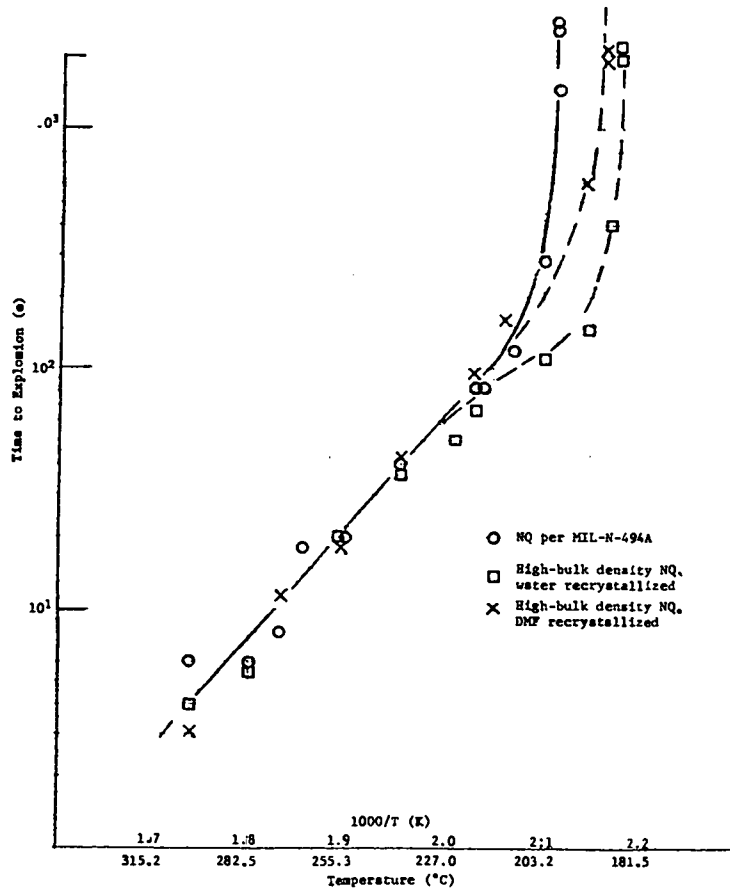
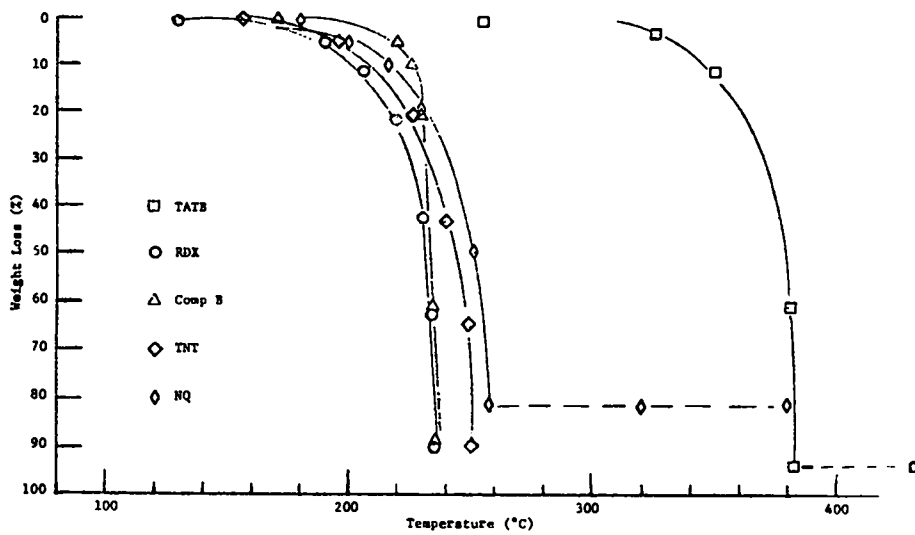Fig. 22.  Time to explosion.



Fig. 23.  TGA, heating rate 10°C/min.

transition. With EXPLO, Jaeger computed the temperature profile in the TNT system as a function of time and space. The EXPLO results were in excellent agreement with the experiment.

## V. CONCLUSIONS

The experimental and computational results obtained for the explosives tested are summarized in Table III. These data indicate that the simple thermal theory of initiation can be used, in almost all cases, to predict the time and temperature-to-ignition. Over the region of heating rates tested, the kinetic source term can be approximated with a zero-order reaction as predicted by Zinn and Rogers.[4]

With the exception of the plastic-bonded NQ formulations, the agreement between the experiment and the calculation, using the kinetics listed in Table I, is within 5%. The fact that we were able to predict the time and temperature-to-ignition with the TNT system is the existence of a stagnant layer of TNT at the hot boundary. It is quite possible that under a set of boundary conditions that would tend to significantly decrease the thickness of the layer, the time-to-ignition would change.

The results obtained with NQ were not predictable with existing kinetics. This indicates that at least one of the terms used to express the energy generation is in error. The most likely term is the heat of reaction, Q.

# TABLE III

## THERMAL RESPONSE

### Summary of Results
### One-Dimensional Slab Configuration

| Material | Time-to-Ignition (min) | | Ignition Temperature (°C) | | Heating Rate (°C/min) |
|---|---|---|---|---|---|
| | Experimental | Calculated | Experimental | Calculated | |
| TNT | 16.0 | 15.5 | 260 | 250 | 13 |
| Comp. B[a] | 17.0 | 17.7 | 210 | 220 | 13 |
| | 11.0 | 10.7 | 225 | 220 | 23 |
| PBX 9501 | 15 | 14.3 | 280 | 275 | 22 |
| PBX 9502 | 18.5 | 18.5 | 340 | 340 | 20 |
| 95 wt% DATB/5 wt% Viton A | 15.0 | 15.7 | 300 | 315 | 20 |
| 95 wt% NQ/5 wt% Estane | I[b] | 18.0 | I[b] | 190 | 10 |
| | I[b] | 10 | I[b] | 190 | 20 |

[a]RDX kinetics

[b]Indeterminate

REFERENCES

1.  H. Hendin and R. McGill, "Rates of Explosive Decomposition of Explosives," I&E Chem. 44, 6, p. 1391 (1952).

2.  J. Zinn and C. L. Mader, "Thermal Ignition of Explosives," J. Appl. Phys. 31, 2, p. 323 (1960).

3.  J. Wenograd, "The Behavior of Explosives at Very High Temperatures," Trans. of the Farady Society 57, p. 1612 (1961).

4.  J. Zinn and R. N. Rogers, "Thermal Initiation of Explosives," J. Phys. Chem. 66, p. 2646 (1962).

5.  E. Catalano, D. Ornellas, E. Wrenn, E. Lee, J. Walton, and R. McGuire, "The Thermal Decomposition and Reaction of Confined Explosives," Sixth Symposium on Detonation, NWC (1976).

6.  C. A. Anderson, "TEPLO: A Heat Conduction Code for Studying Thermal Explosions in Laminar Composites," Los Alamos Scientific Laboratory report LA-4511 (November 1970).

7.  R. N. Rogers, "Thermochemistry of Explosives," Thermochemica Acta 11, pp. 131-139 (1975).

8.  A. J. B. Robertson, "Thermal Decomposition of Explosives, Part II," Trans. of the Farady Society 45, p. 85 (1948).

9.  R. N. Rogers, Los Alamos Scientific Laboratory, personal communication, June 1976.

10. D. L. Jaeger, "EXPLO: Explosives Thermal Analysis Computer Code," Los Alamos Scientific Laboratory report LA-6949-MS (January 1978).

APPENDIX

REACTIVE HEAT-TRANSFER CALCULATIONS WITH MODIFIED TEPLO

The TEPLO code was modifed to allow the use of a series of time-dependent thermal boundary conditions and to study the transient heat conduction and exothermic decomposition in a variety of high explosives subjected to time-dependent boundary temperatures. The changes in the code allow it to be used with the original fixed boundary conditions or with up to 10, linear, time-dependent flux or temperature boundaries.

To use the code with the time-dependent thermal boundary conditions, only a slight change was made to the boundary condition card, and immediately following it, a card was added to the deck for each different boundary condition. The remainder of the input cards are as described in LA-4511.

The modifed input is as follows:

Boundary Condition Card = Format (4E8·3, I4)

### Columns

| | |
|---|---|
| 1-8 | Inner boundary temperature in K at initial time |
| 9-16 | Outer boundary temperature in K at initial time |
| 17-24 | Inner boundary flux in cal/cm$^2$-s at initial time |
| 25-32 | Outer boundary flux in cal/cm$^2$-s at initial time |
| 33-36 | Number of additional boundary conditions |

Additional Boundary Condition Cards = Format (4E8·3)

### Columns

| | |
|---|---|
| 1-8 | Time (s) at end of inner boundary condition |
| 9-16 | Time (s) at end of outer boundary condition |
| 17-24 | Flux (cal/cm$^2$-s) or temperature (K) at end of inner boundary condition |
| 25-32 | Flux (cal/cm$^2$-s) or temperature (K) at end of boundary condition |

If columns 33-36 in the boundary condition card are left blank or coded zero, the code will use the constant boundary conditions given for the initial time (t = 0). The number of additional boundary condition cards must equal the value given in these columns. The code implements each of the time-dependent, thermal boundary conditions by interpolating a linear heat or temperature input curve, with the times and conditions from the previous card as the first point on the curve and the times and conditions given on that card as the last point.

When the time given on one boundary condition card has been reached or exceeded, the heating curve defined by the next card is used. If a new boundary condition is not defined for either the inner or outer boundary, the code will use the previous boundary value specified until a new temperature or flux is defined or for the duration of the run. Because the inner and outer boundary conditions are independent of each other, a number of options

are available: (1) a flux input may be used at one boundary and a variable temperature definition on the other; (2) one boundary condition can be varied while holding the other constant; or (3) both boundary conditions can be varied at the same time.

Figures 1-A and 2-A show the maximum temperature-time plots of the first and last layers, respectively, of a four-layer cross section using the five boundary condition cards listed below.

| Card | Column Numbers | | | | |
|------|------|------|-------|-------|-------|
| No. | 1-8 | 9-16 | 17-24 | 25-32 | 33-36 |
| 1 | 500. | 400. | | | 4. |
| 2 | 20. | 40. | 600. | 700. | |
| 3 | 60. | 50. | 800. | 900. | |
| 4 | 100. | 200. | 400. | 1000. | |
| 5 | 300. | | 300. | | |

Layers 1 and 4 represent thin metal sheets with high thermal conductivities placed outside thick layers of insulating material with extremely low conductivities. Thus, Figs. 1-A and 2-A closely represent the changes to the boundary conditions as implemented by the code. Note that time is plotted on a log scale so that the curves are not composed of a series of straight lines as they would be if a linear time scale were used.
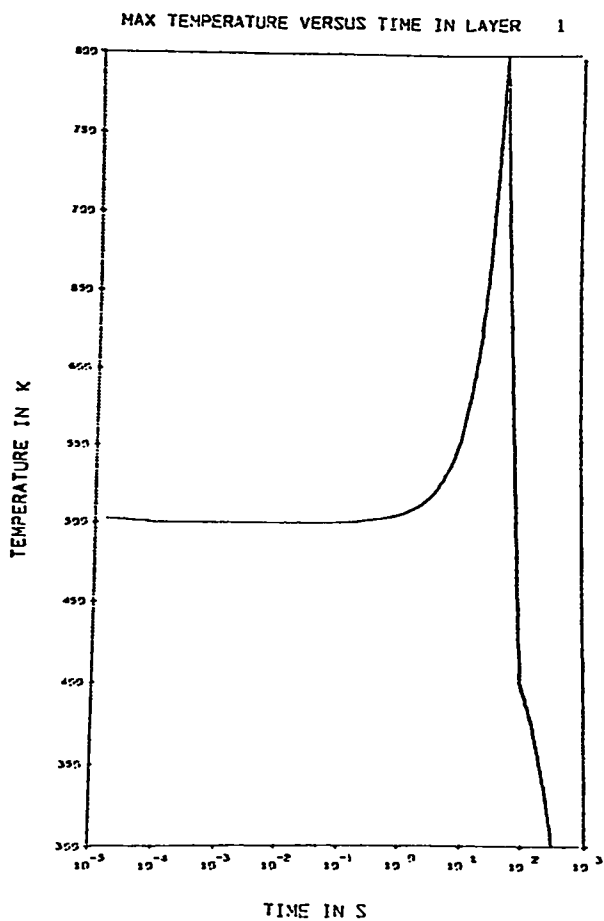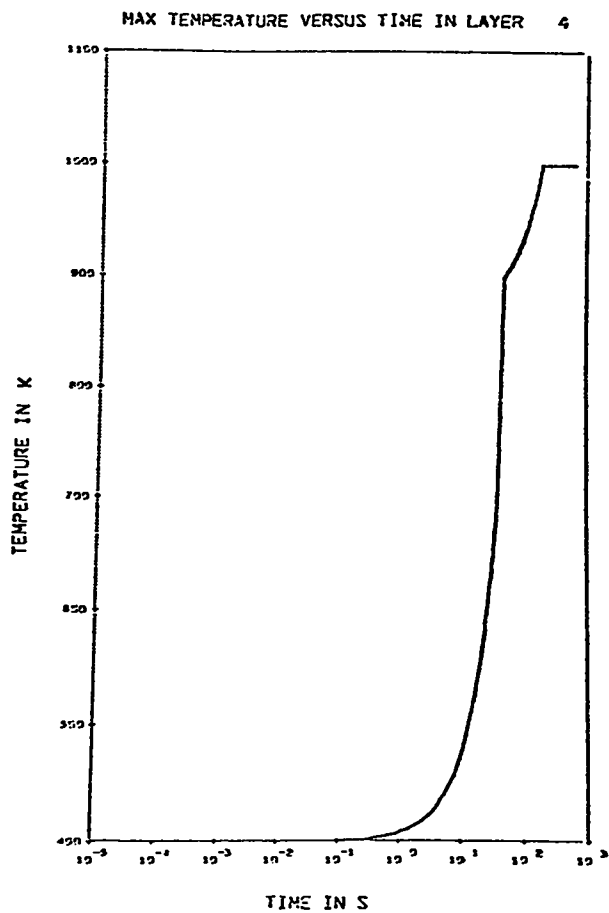
Fig. 1-A.   Temperature at the inner
boundary.



Fig. 2-A.   Temperature at the outer
boundary.

# SPECIAL DISTRIBUTION

| | No. of Copies | | No. of Copies |
|---|---|---|---|
| HQ USAF/RDQRM<br>Washington, DC 20330 | 1 | HQ TAC/INAT<br>Langley AFB, VA 23665 | 1 |
| HQ USAF/XOXFCM<br>Washington, DC 20330 | 1 | HQ SAC/LGWC<br>Offutt AFB, NE 68113 | 1 |
| HQ USAF/SAMI<br>Bolling AFB<br>Washington, DC 20332 | 1 | HQ SAC/NRI (Stinfo Library)<br>Offutt AFB, NE 68113 | 1 |
| AFSC/IGFG<br>Andrews AFB<br>Washington, DC 20331 | 1 | Central Intelligence Agency<br>CRL/ADD/Publications<br>Washington, DC 20505 | 1 |
| Directorate of Strike Armament<br>HQ AFSC/SDZA<br>Andrews AFB<br>Washington, DC 20334 | 1 | AFWL/LR<br>Kirtland AFB, NM 87117 | 1 |
| HQ AFSC/DICAW<br>Andrews AFB<br>Washington, DC 20331 | 1 | AFWL/SUL<br>Technical Library<br>Kirtland AFB, NM 87117 | 1 |
| AFML/DO/AMIC<br>Wright-Patterson AFB, OH 45433 | 1 | AUL/LSE 71-209<br>Maxwell AFB, AL 36112 | 1 |
| AFIT/LD<br>Building 640 Area B<br>Wright-Patterson AFB, OH 45433 | 1 | Redstone Scientific Information Ctr.<br>DRDMI-TBD<br>US Army Missile R&D Command<br>Redstone Arsenal, AL 35809 | 1 |
| ASD/ENFLA<br>Attn: W. Hartley<br>Wright-Patterson AFB, OH 45433 | 1 | Commander<br>US Army Armament R&D Command<br>Attn: DRDAR-TSS 59<br>Dover, NJ 07801 | 1 |
| AFFDL/FES<br>Attn: C. D. Cruze<br>Wright-Patterson AFB, OH 45433 | 1 | Naval Surface Weapons Center<br>Attn: Code G-14<br>Dahlgren, VA 22448 | 1 |
| ASD/ENESH<br>Attn: S. Johns<br>Wright-Patterson AFB, OH 45433 | 1 | Naval Surface Weapons Center<br>White Oak Library<br>White Oak, Silver Spring, MD 20910 | 2 |
| ASD/XRP<br>Wright-Patterson AFB, OH 45433 | 1 | NSWC/White Oak Laboratory<br>Attn: J. F. Leahy<br>R-12, Building 613<br>Silver Spring, MD 20910 | 1 |
| TAC/DRAR<br>Langley AFB, VA 23665 | 1 | | |

|  | No. of Copies |  | No. of Copies |
|---|---|---|---|
| Commanding Officer<br>Naval Weapons Station<br>Code 2034<br>Yorktown, VA   23691 | 2 | AFATL/DLDE<br>Eglin AFB, FL   32542 | 10 |
| | | AFATL/DL<br>Eglin AFB, FL   32542 | 1 |
| Commander (Code 233)<br>Information Science Division<br>Naval Weapons Center<br>China Lake, CA   93555 | 1 | AFIS/INTI<br>Washington, DC   20330 | 1 |
| Lawrence Livermore Laboratory<br>Attn: Dr. R. McGuire/L-324<br>P.OL Box 808<br>Livermore, CA   94550 | 1 | HQ USAFE/DOQ<br>APO New York   09012 | 1 |
| | | HQ PACAF/DOOFQ<br>Hickam AFB, HI   96853 | 2 |
| Lawrence Livermore Laboratory<br>Attn: Dr. M. Finger<br>P.O. Box 808<br>Livermore, CA   94550 | 1 | IPAC (Library)<br>Box 38<br>Camp H. M. Smith, HI   96861 | 2 |
| Accessions Division (DDC-TC)<br>Defense Documentation Center<br>Building 5<br>Cameron Station<br>Alexandria, VA   22314 | 1 | Director<br>USA Tradoc Sys. Anal. Activity<br>Attn: ATAA-SL (Technical Library)<br>White Sands Missile Range, NM 88002 | 1 |
| OO-ALC/MMWM<br>Hill AFB, UT   84406 | 2 | Commanding Officer<br>Naval Weapons Support Center<br>Attn: Code 3031<br>Crane, IN   47522 | 3 |
| AFATL/DLODL<br>Eglin AFB, FL   32542 | 2 | | |